nature water

Article

https://doi.org/10.1038/s44221-023-00113-5

Shielding effect enables fast ion transfer through nanoporous membrane for highly energy-efficient electrodialysis

Received: 25 July 2022

Accepted: 1 July 2023

Published online: 3 August 2023

Check for updates

Jiuyang Lin[1,2,3,4] ✉, Wenyuan Ye[5] ✉, Shuangling Xie[4], Jiale Du[4], Riri Liu[4], Dong Zou[6], Xiangyu Chen[4], Zijian Yu[4], Shengqiong Fang[4], Elisa Yun Mei Ang[7], William Toh[8], Dan Dan Han[9], Teng Yong Ng[8], Dong Han Seo[10], Shuaifei Zhao[11], Bart Van der Bruggen[12], Ming Xie[13] ✉ & Young Moo Lee[6] ✉

A key to sustainable management of saline organic-rich wastewaters is to precisely fractionate organic components and inorganic salts (NaCl) as individual resources. Conventional nanofiltration and electrodialysis processes suffer from membrane fouling and compromise the fractionation efficacy. Here we develop a thin-film composite nanoporous membrane via co-deposition of dopamine and polyethyleneimine as a highly anion-conducting membrane. Experimental results and molecular dynamics simulations show that co-deposition of dopamine and polyethyleneimine effectively tailors the membrane surface properties, intensifying the charge shielding effect and enabling fast anion transfer for highly efficient electrodialysis. The resulting nanoporous membrane exhibits unprecedented electrodialytic fractionation of organics and NaCl with negligible membrane fouling, dramatically outperforming state-of-the-art anion exchange membranes. Our study sheds light on facile design of high-performance anion-conducting membranes and associated new mass transport mechanisms in electrodialytic separation, paving the way for sustainable management of complex waste streams.

To advance net-zero carbon emission for a circular economy, current wastewater treatment processes urgently need a paradigm shift from conventional contaminant removal to resource recovery, for example, energy, nutrients, biomass and other high value-added by-products that are beyond water reclamation by reverse osmosis[1–5]. One grand challenge in wastewater treatment is the management of saline organic-rich waste streams produced in a wide range of industrial sectors, such as textile processing, tanneries, food processing, the oil and gas

[1]Ganjiang Innovation Academy, Chinese Academy of Sciences, Ganzhou, China. [2]Jiangxi Province Key Laboratory of Cleaner Production of Rare Earths, Ganzhou, China. [3]Key Laboratory of Rare Earths, Chinese Academy of Sciences, Ganzhou, China. [4]College of Environment and Safety Engineering, Fuzhou University, Fuzhou, China. [5]Fujian Provincial Key Laboratory of Soil Environmental Health and Regulation, College of Resources and Environment, Fujian Agriculture and Forestry University, Fuzhou, China. [6]Department of Energy Engineering, College of Engineering, Hanyang University, Seoul, Republic of Korea. [7]Engineering Cluster, Singapore Institute of Technology, Singapore, Singapore. [8]School of Mechanical and Aerospace Engineering, Nanyang Technological University, Singapore, Singapore. [9]College of Mechanical and Vehicle Engineering, Hunan University, Changsha, China. [10]Institute of Energy Materials and Devices, Korea Institute of Energy Technology (KENTECH), Naju, Republic of Korea. [11]Institute for Frontier Materials, Deakin University, Geelong, Victoria, Australia. [12]Process Engineering for Sustainable Systems (ProcESS), Department of Chemical Engineering, KU Leuven, Leuven, Belgium. [13]Department of Chemical Engineering, University of Bath, Bath, UK. ✉e-mail: jylin@gia.cas.cn; ye0508@126.com; m.xie2@bath.ac.uk; ymlee@hanyang.ac.kr

industry, paper mills and pharmaceutical manufacturing[6–9]. Therefore, it is important to effectively fractionate organic and inorganic salts (for example, NaCl) using innovative and advanced separation technology to sustainably recover precious resources from these saline organic-rich waste streams[10].

Membrane-based separation technologies offer opportunities to effectively manage these saline organic-rich waste streams. For instance, nanofiltration is among the most widely used pressure-driven membrane technologies to sieve organics with molecular weights (MWs) of 200–1,000 Da and inorganic salts from the saline organic-rich waste streams based on the synergistic effects of size exclusion and electrostatic repulsion using the nanoporous thin-film composite (TFC) membranes, which retain the organics but partially allow the transmission of inorganic salts[11–16]. However, the elevated osmotic pressure, membrane fouling and cake-enhanced concentration polarization experienced in the pressure-driven nanofiltration process induce detrimental membrane flux decline, thereby minimizing the separation efficiency of the organic and inorganic salts[17–19]. Additionally, the pressure-driven nanofiltration–diafiltration procedure should be implemented with high consumption of pure water to achieve the fractionation of organic and inorganic salts, which inevitably suffers from a considerable loss of the target organics and thus reduces the system productivity[10,20].

As an alternative approach to nanofiltration, electrodialysis is proposed as a route for desalinating the saline organic-rich wastewaters, which allows cations and anions to be transferred through cation exchange membranes (CEMs) and anion exchange membranes (AEMs) under a direct current electric field[21–23]. Nevertheless, most organic compounds with negative charges in the saline organic-rich wastewaters migrate to the AEMs via electrostatic attraction, which deteriorates membrane fouling during the electrodialysis process[24–26], significantly limiting the transfer efficiency of the anions and jeopardizing the fractionation of the organic and inorganic salts.

By integrating the technical merits and advantages of the pressure-driven nanofiltration (nanoporous membranes, NPMs) and the electrodialysis process (electro-driven process with low/zero pressure), we herein devised a new electro-driven membrane system using TFC nanoporous polyamide (PA) membranes (with a molecular weight cut-off (MWCO) of 200–1,000 Da) as anion-conducting membranes (ACMs) to replace the AEMs used in conventional electrodialysis. This strategy both alleviates membrane fouling and accelerates ion transfer. Due to the nanoporous structure of the membranes, the anions can migrate through the nano-channels of the TFC PA membranes under a direct electric field. However, nanoporous TFC PA membranes are highly negatively charged and can significantly impede the anion transfer through electrostatic repulsion, and thus deteriorate the desalination efficiency under the current field. Therefore, it is vital to molecularly tailor the surface properties of the nanoporous PA membranes for intensifying the charge shielding effect, thus enhancing the anion transfer and solute selectivity while effectively separating the organics without fouling. To modulate the membrane surface properties, a bio-inspired polydopamine (PDA)-based coating on PA nanofiltration membrane is proposed as a novel and scalable strategy for constructing a multifunctional surface for enhanced membrane performance[27,28]. However, there are limited examples of PDA-coated NPMs in the electro-driven membrane process with a couple of applications in pressure-driven membrane filtration or superhydrophilic surface modifications[29,30].

In this Article, we present the design of surface-engineered, highly anion-conducting, anti-fouling TFC NPMs featuring a facile co-deposition of dopamine and polyethyleneimine (PEI) for effective electrodialytic fractionation of the organic and inorganic salts from saline organic-rich wastewaters (Fig. 1a,b). Co-deposition of dopamine and PEI effectively tunes the surface properties of the PDA/PEI-coated TFC NPMs as ACMs, which both enhances the solute selectivity (as is evident from the experimental data) and manifests an ion shielding effect for fast electrodialytic anion transfer as demonstrated by molecular dynamics (MD) simulation. The optimal PDA/PEI-coated TFC NPM exhibits over 99.3% desalination efficiency and more than 99.1% recovery of organics for highly effective electrodialytic fractionation of various organics/NaCl mixed solutions. Finally, we show that PDA/PEI-coated TFC NPMs are exceptionally stable to achieve impressive fractionation performance with negligible fouling propensity in an 18-cycle electrodialytic separation operation. This highlights the practicability of surface-engineered TFC NPMs as advanced ACMs in one-step electro-driven fractionation of the organic and inorganic salts from complex saline organic-rich wastewaters for a sustainable circular economy.

Molecular design and characterization of the TFC NPMs

A loose poly(piperazine amide) TFC NPM with a MWCO of 682 ± 17 Da was used as the substrate for fabrication of highly anion-conductive TFC NPMs via co-deposition of dopamine and PEI at pH 8.5 (Fig. 1a). The coated TFC NPMs were exposed to the dopamine/PEI solution at different durations, that is, 6, 12, 18, 24, 30 and 36 h, and were denoted as NPM-1, NPM-2, NPM-3, NPM-4, NPM-5 and NPM-6, respectively. Meanwhile, the loose TFC NPM substrate was referred to as NPM-0 and was used as a control. The surface colour of the coated TFC membranes changed from a white pattern to a light-yellow pattern and finally to a brown pattern (Supplementary Fig. 1), demonstrating the successful and homogeneous polymerization of dopamine and PEI on the membrane surfaces. This was further confirmed by scanning electron microscopy (SEM) images (Supplementary Fig. 2). X-ray photoelectron spectroscopy analysis proved that the co-deposition of dopamine and PEI on the loose NPM substrate was induced through Schiff base or/and Michael addition reactions (Supplementary Figs. 3 and 4). Such a PDA/PEI complex coating enables an increase in the thickness of selective layer for the PDA/PEI-coated NPMs from 87.5 ± 8.5 nm (NPM-0) to 135.0 ± 12.6 nm (NPM-6), as demonstrated by atomic force microscopy (AFM) measurements (Supplementary Figs. 5 and 6).

Furthermore, surface properties (that is, hydrophilicity, surface charges, specific areal electric resistance and pore size) of the PDA/PEI-coated NPMs can be precisely tuned via co-deposition of dopamine and PEI on the loose NPM substrate (Fig. 1e–h). In particular, the surfaces of the coated NPMs become more hydrophilic and less negatively charged (Fig. 1e,f) due to the intercalation of the PEI molecules with positive charges through co-polymerization with dopamine. Such a PDA/PEI complex coating can minimize the specific areal electric resistance of the coated NPMs through reduced surface negative charge density (Fig. 1g). As expected, the specific areal electric resistance of the coated TFC NPMs was reduced from 10.47 ± 0.43 (NPM-0) to 5.69 ± 0.13 Ω cm^2 (NPM-6) after a 36 h deposition of the PDA/PEI complex layer, which is beneficial for enhanced ion conductivity under an electric field. Simultaneously, the pore size of the coated TFC NPMs was significantly reduced since the PDA/PEI complex coating can sufficiently bridge the cavity structure of the loose NPM substrate, which can enhance the retention of organics (as reflected by the reduction in MWCO and effective mean pore size in Fig. 1h, Supplementary Fig. 7 and Supplementary Table 3). This change in surface properties impart the PDA/PEI-coated TFC NPMs with enhanced selectivity of the organics over inorganic salts (that is, NaCl).

Pressure-driven separation performance of the TFC NPMs

Pressure-driven filtration was performed to illustrate the solute selectivity of the PDA/PEI-coated NPMs between inorganic salts (that is, NaCl) and organics. In this study, four antibiotics, that is, ceftriaxone sodium, cefotaxime sodium, carbenicillin disodium and ampicillin sodium, were selected as the model organics. The rejection of

https://doi.org/10.1038/s44221-023-00113-5

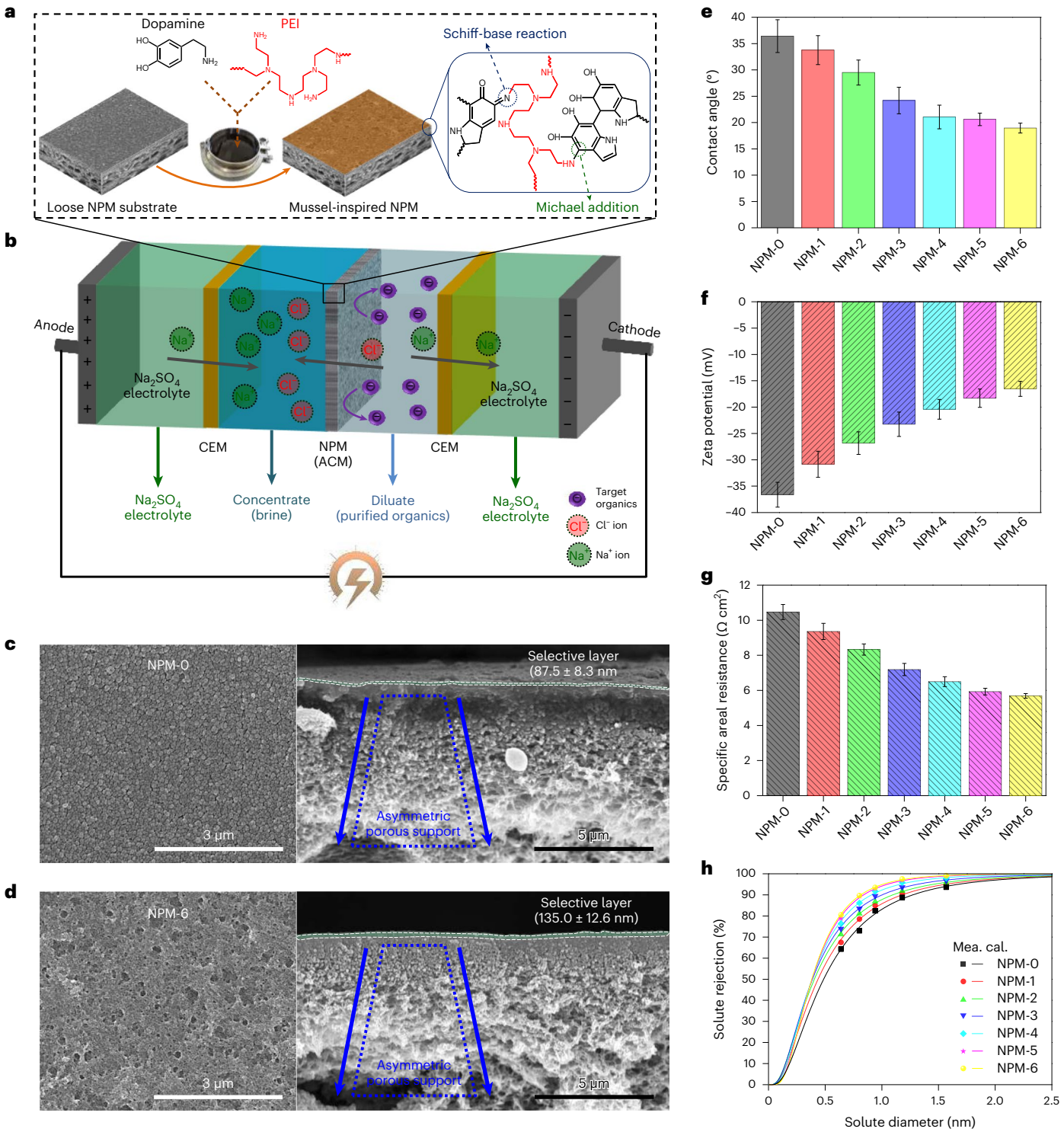

Fig. 1 | Design and characterization of surface-engineered TFC NPMs as ACMs for electrodialytic fractionation of organics and NaCl. a, Schematic diagram of dopamine-based bio-inspired coating of TFC NPM. **b**, Stack configuration of novel electro-driven separation process using the PDA/PEI-coated NPMs as ACMs for one-step electrodialytic fractionation of organics and NaCl. **c**, Surface and cross-sectional SEM images of the loose TFC NPM substrate. **d**, Surface and cross-sectional SEM images of the TFC NPM after 36 h PDA/PEI coating (NPM-6). **e**, Surface hydrophilicity of the TFC NPMs. **f**, Zeta potential of the TFC NPMs. **g**, Specific areal electric resistance of the TFC NPMs. **h**, Relationship between MWs of poly(ethylene glycol) polymers and their rejection for the TFC NPMs where the symbols represent measured data and the curves modelled using Equation S4 in the Supplementary Information. Error bars represent standard deviation from triple measurements of duplicate samples.

antibiotics for the PDA/PEI-coated NPMs increased when the coating duration was extended (Supplementary Fig. 8a), which was ascribed to the reduction in pore size of the PDA/PEI-coated NPMs, thereby enhancing the rejection of organics via size exclusion effect. For instance, the NPM-6 membrane exhibited rejection of 98.5 ± 0.2% to ampicillin sodium, markedly outperforming the pristine loose NPM-0 substrate (88.9 ± 0.5%). Conversely, the rejection of NaCl for the PDA/PEI-coated NPMs unexpectedly decreased with increasing coating duration

https://doi.org/10.1038/s44221-023-00113-5

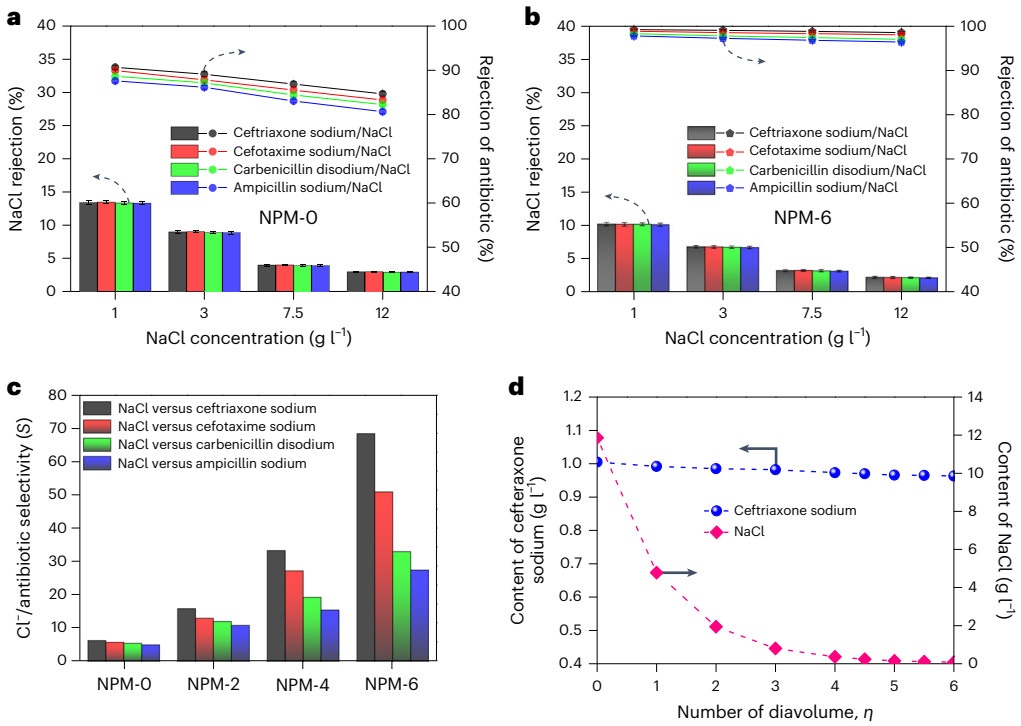

Fig. 2 | Pressure-driven separation of antibiotic/NaCl mixed solutions using NPMs. a,**b**, Rejection of antibiotics and NaCl for the NPM-0 and NPM-6 membranes, respectively, when filtering various antibiotic/NaCl mixed solutions. **c**, Selectivity between NaCl and antibiotic for the NPM-0, NPM-2, NPM-4 and NPM-6 membranes when filtering various antibiotic/NaCl mixed solutions with a NaCl concentration of 12 g l^{-1}. **d**, Content of antibiotic and NaCl in the feed during the constant-volume nanofiltration-based diafiltration using the NPM-6 membrane for fractionation of antibiotic and NaCl from a ceftriaxone sodium/NaCl mixed solution. Error bars represent standard deviation from triple measurements of duplicate filtration experiments.

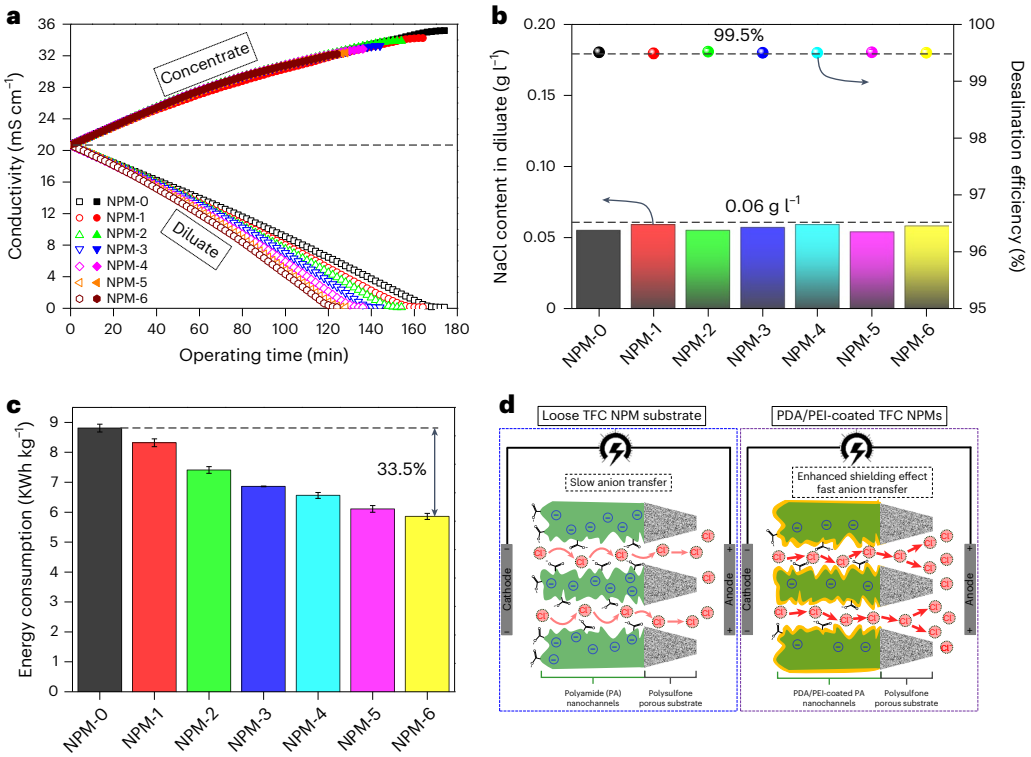

Fig. 3 | Electrodialytic separation performance of the PDA/PEI-coated TFC NPMs in pure NaCl solution (about 12.0 g l^{-1}) at a current of 0.5 A. a, Evolution of conductivity in both concentrate and diluate. **b**, NaCl concentration in the diluate and desalination efficiency. **c**, Energy consumption. **d**, Illustration of anion transfer pathway through the TFC NPMs during the electrodialytic separation. Error bars represent standard deviation from triple measurements.

https://doi.org/10.1038/s44221-023-00113-5

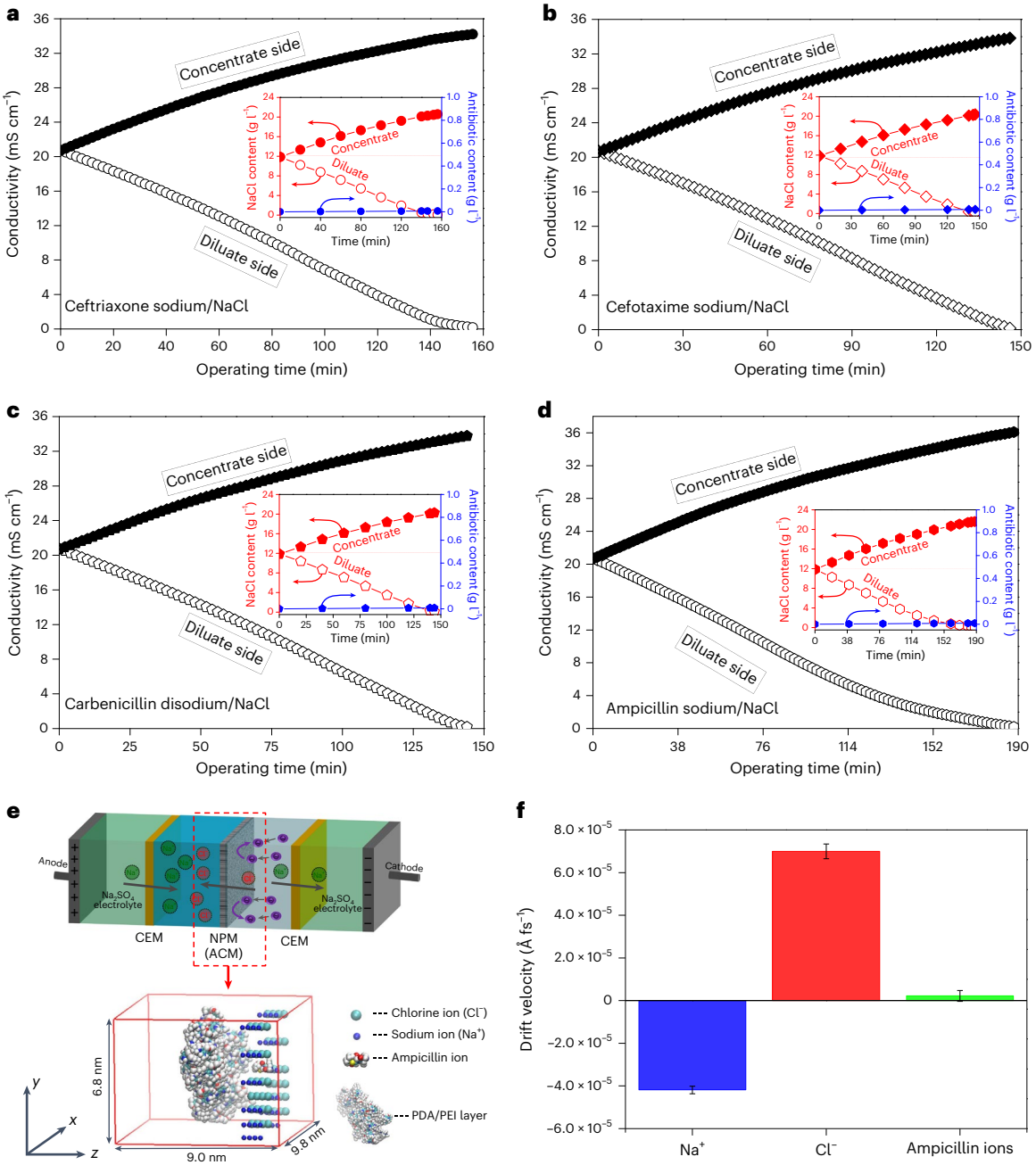

Fig. 4 | Electro-driven separation of antibiotic/NaCl mixed solutions using PDA/PEI-coated TFC NPMs (that is, NPM-6) as ACMs. a–**d**, Evolution of conductivity in the concentrate and diluate during fractionation of antibiotic and NaCl in the (**a**) ceftriaxone sodium/NaCl, (**b**) cefotaxime sodium/NaCl, (**c**) carbenicillin disodium/NaCl and (**d**) ampicillin sodium/NaCl mixed solutions, respectively, by electro-driven process using the NPM-6 membrane at a current of 0.5 A (inset: content of NaCl in both concentrate and diluate and content of antibiotic in the concentrate). **e**, Details of the MD simulation domain (note that water molecules are not shown in the simulation domain for clarity). **f**, Drift velocity of Na^+, Cl^- and ampicillin ions with samples collected at every 200 fs interval for the last 15 ns across three runs for MD system. The error bars represent the standard deviation from three simulation runs.

(Supplementary Fig. 8b). This could be attributed to the reduction in negative surface charge density of the coated NPMs (reflected by the change in zeta potential in Fig. 1f), leading to a diminished electrostatic repulsion for fast NaCl transmission[31–33].

Both organic and inorganic salts (that is, NaCl) co-exist in real saline organic-rich solutions. The presence of inorganic salts would significantly affect the separation behaviour of the TFC NPMs, which enhances the shielding effect for reduced solute retention[7,34]. Specifically, the rejection of organics for the pristine loose NPM substrate (that is, NPM-0) significantly decreased with increasing NaCl concentration, yielding a reduced selectivity between NaCl and antibiotics in the antibiotic/NaCl mixed solutions as feed (Fig. 2a). After coating of the PDA/PEI complex layer, the coated TFC NPMs exhibited increasing rejection towards the organics in the same antibiotic/NaCl mixed solutions (Fig. 2b and Supplementary Fig. 9). The deleterious impact of the presence of NaCl on the rejection of organics was minimized for the PDA/PEI-coated NPMs with a 36 h coating duration (that is, NPM-6). The rejection of all the antibiotics for the NPM-6 membrane was marginally diminished with increasing NaCl concentrations since the size exclusion effect of the NPM-6 membrane was maximized with

a remarkable reduction in its pore sizes. This enabled an impressive increase in the selectivity of NaCl and antibiotics for their potential effective fractionation (Fig. 2c). For instance, the selectivity of NaCl and ampicillin sodium in the antibiotic/NaCl mixed solution through the NPM-6 membrane reached 27.4, which was much higher than that (that is, 5.0) of the pristine loose NPM-0 substrate during the pressure-driven nanofiltration procedure (Fig. 2c).

Although the PDA/PEI-coated NPMs showed enhanced selectivity between NaCl and antibiotics, a constant-volume nanofiltration-based diafiltration procedure using the NPM-6 membrane should be implemented for fractionation of antibiotics and NaCl from the antibiotic/NaCl mixed solutions (Fig. 2d and Supplementary Fig. 10). The concentration of NaCl in all the antibiotic/NaCl mixed solutions significantly decreased with increasing diavolume number during diafiltration. This is because the low overall rejection of NaCl (<30%) for the NPM-6 membrane allowed fast penetration of NaCl through the membrane (Supplementary Figs. 11a–14a). When the diavolume number increased to 5.9–6.0, the concentration of NaCl in all the antibiotic/NaCl mixed solutions was reduced from 11.9 g l^{-1} to 0.08 g l^{-1}, resulting in a desalination efficiency of 99.3–99.4% (Supplementary Table 4). On the other hand, the NPM-6 membrane with a smaller pore size can effectively retain the antibiotics even after diafiltration of the antibiotic/NaCl mixed solutions. However, as the diavolume number increased, the antibiotics were still able to penetrate through the NPM-6 membrane along with the nanofiltration permeate. For antibiotics with a lower MW (for example, ampicillin sodium), a moderate amount of the antibiotics transported from the feed to the permeate, even though the NPM-6 membrane exhibited antibiotic rejections over 96%. Consequently, the loss of ceftriaxone sodium, cefotaxime sodium, carbenicillin disodium and ampicillin sodium from the feed to the permeate side reached 4.18%, 6.27%, 8.98% and 11.47% (Supplementary Figs. 11b–14b), respectively. Therefore, the constant-volume nanofiltration-based diafiltration procedure driven by pressure cannot sufficiently recover antibiotics during the fractionation of antibiotics and NaCl from the antibiotic/NaCl mixed solutions (Supplementary Table 4).

Electro-driven separation performance of the coated TFC NPMs

The PDA/PEI-coated NPMs were used as ACMs to replace the AEMs in the conventional electrodialysis for evaluating their electro-driven separation performance (Fig. 3). During the electro-driven membrane-based separation, sufficient desalination of the pure NaCl solutions can be achieved using the PDA/PEI-coated NPMs as ACMs (Fig. 3a). For instance, the NPM-6 membrane yielded a desalination efficiency of 99.5% for the pure NaCl solution with a minimal energy consumption of 5.86 ± 0.10 kWh kg^{-1} during 124 min of operation (Fig. 3b,c), which was comparable to commercial AEMs (Supplementary Fig. 15b,d,e). This demonstrates an impressive anion transfer capacity of the PDA/PEI-coated NPMs for desalination (Fig. 3d). The remarkable anion transfer enhancement of the PDA/PEI-coated TFC NPMs was mainly attributed to two factors: (1) sufficient nano-channels and short ion diffusion pathways caused by the intrinsically thin selective layer of the PDA/PEI-coated TFC NPMs that enable effective anion transfer under the electric field; (2) the reduced negative charge density of the PDA/PEI-coated TFC NPMs intensifies the shielding effect, and thus lowers the energy barrier (that is, electrostatic repulsion) between anions and the membrane surface for anion transfer. Although commercial AEMs with a non-porous structure generally have abundant positively charged quaternary ammonium group sites, their thickness is in the order of hundreds of micrometres, which provides a longer ion diffusion pathway for anion transfer (Supplementary Fig. 15c). Therefore, such an improvement in anion conductivity of the PDA/PEI-coated TFC NPMs provides an important conceptual framework for the facile design of cost-effective ACMs.

Table 1 | Performance overview of electro-driven separation process using PDA/PEI-coated NPM (that is, NPM-6) for one-step fractionation of antibiotics and NaCl

Organics/NaCl mixtures	NaCl content in diluate (g l^{-1})	Desalination efficiency (%)	Recovery of antibiotics (%)
Ceftriaxone sodium/NaCl	0.076	99.36	99.28
Cefotaxime sodium/NaCl	0.08	99.33	99.26
Carbenicillin disodium/NaCl	0.083	99.30	99.21
Ampicillin sodium/NaCl	0.078	99.35	99.11

In addition, we examined the fractionation efficacy of the PDA/PEI-coated TFC NPMs (that is, NPM-6) in the antibiotic/NaCl mixed solutions under an electric field. Sufficient anion transfer capacity imparted the NPM-6 membrane with a desalination efficiency of >99.3% for all the antibiotic/NaCl mixed solutions (Fig. 4a–d). More importantly, only a trace amount of organics (<10 ppm) passed into the concentrate side, suggesting sufficient fractionation of all the antibiotics (that is, ceftriaxone sodium, cefotaxime sodium, carbenicillin disodium and ampicillin sodium) and NaCl. Unprecedentedly high recovery efficiencies (>99.1%) of all the antibiotics were obtained from the antibiotic/NaCl mixed solutions (Table 1) during the electro-driven separation. Therefore, the PDA/PEI-coated TFC NPMs with a thin nanoporous layer offer both nano-channels for effective, unperturbed anion transfer, and they substantially retain organics via an enhanced size exclusion effect, achieving an extremely high permselectivity between NaCl and antibiotic (that is, up to 21,407 between NaCl and ceftriaxone sodium) (Supplementary Fig. 16), and thus leading to a one-step fractionation of the organics and NaCl under an electric field. Furthermore, such an electro-driven separation process using the surface-engineered TFC NPMs (that is, NPM-6) as ACMs markedly outperformed the pressure-driven diafiltration process using the NPM-6 membrane as a nanofiltration membrane (Supplementary Table 4) for fractionation of the organics and NaCl in terms of organic recovery and water consumption.

To challenge long-term viability of the PDA/PEI-coated NPMs for fractionation of the antibiotic/NaCl mixed solutions, the fouling propensity of the NPM-6 membrane based on an 18-cycle electro-driven separation operation was investigated (Fig. 5). Nearly identical performance in each cycle for fractionation of antibiotics (that is, ceftriaxone sodium) and NaCl was observed in this 18-cycle electro-driven separation operation, featuring the superior long-term stability of TFC NPM with a consistently high desalination efficiency (99.3–99.4%) over several cycles (Fig. 5a,b). Such an extremely low fouling propensity of the NPM-6 membrane was further demonstrated by the modest increase in its specific areal electric resistance after the 18-cycle electro-driven separation operation (Fig. 5b). In summary, the outstanding overall fractionation performance of the NMP-6 membrane can be explained by its relatively small pore size, which sufficiently retained the organics and impeded the penetration of the organics into the inner pore structure from the blockage of its nano-channels, eventually guaranteeing effective anion transfer and recovery of the organics (>99.2%) (Fig. 5c,d). Moreover, the negatively charged surface of the NPM-6 membrane aided in electrostatic repulsion of the organics to some extent, lowering the fouling propensity. Expectedly, the NPM-6 membrane also exhibited a remarkable fouling resistance against humic acid even in the humic acid/NaCl mixed solution with an elevated salinity (~50g l^{-1} NaCl) during a four-cycle electrodialytic separation operation, which can be reflected by the nearly identical decay in conductivity of the humic acid/NaCl mixed solution (Supplementary Fig. 17a) in the diluate for each cycle. Moreover, the NPM-6 membrane yielded an impressive fractionation of humic acid and NaCl in the humic acid/NaCl mixed solution

https://doi.org/10.1038/s44221-023-00113-5

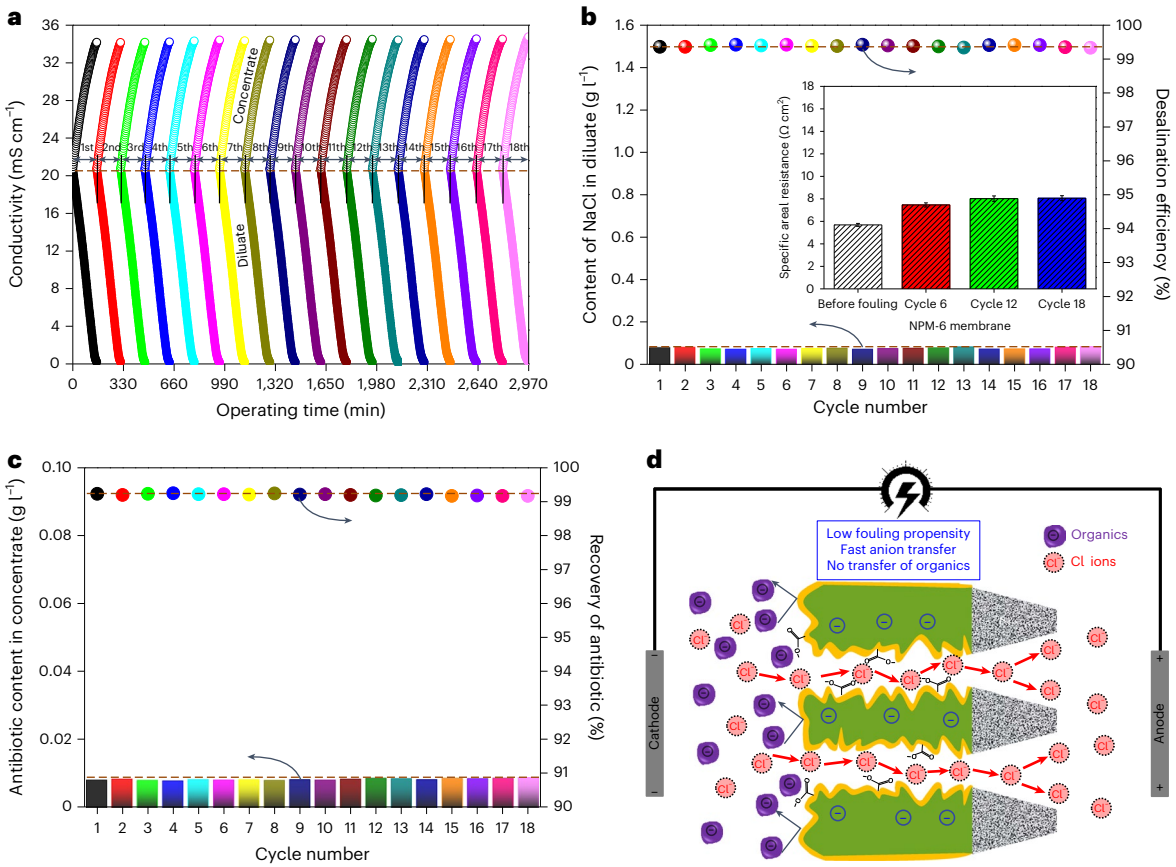

Fig. 5 | Eighteen-cycle electrodialytic separation process using the NPM-6 membrane as ACM for fractionation of the ceftriaxone sodium/NaCl mixed solution (salinity ~12 g l^{-1} NaCl). a, Evolution of conductivity in the concentrate and diluate. **b**, Content of NaCl in the diluate and its desalination efficiency (inset: specific areal electric resistance of NPM-6 before and after fouling). **c**, Content of ceftriaxone sodium in the concentrate and its recovery rate. **d**, Schematics of anion transfer of the NPM-6 membrane during electrodialytic fractionation of ceftriaxone sodium and NaCl.

with a desalination efficiency of 99.2% (Supplementary Fig. 17b) and humic acid recovery of 99.6–99.7% (Supplementary Fig. 17c).

Discussion

Unlike the AEMs with positively charged group sites, the PDA/PEI-coated TFC NPMs provide enhanced electrodialytic transfer of anions by intensifying the charge shielding effect. Furthermore, we performed MD simulations of ion transfer to further elucidate the mass transport mechanism of the PDA/PEI-coated TFC NPMs in electrodialysis (Fig. 4e,f and Supplementary Movies 1–3). When the electric field was applied across the PDA/PEI-coated TFC NPMs, we observed that Cl^- ions move towards the anode through the PDA/PEI-coated NPMs, while Na^+ ions move towards the cathode (Supplementary Movies 1 and 2). Additionally, the calculated negative drift velocity of Cl^- ions and positive drift velocity of Na^+ ions (Fig. 4f) demonstrate the moving direction of Cl^- and Na^+ ions under the electric field. Although there is a weak electrostatic repulsion between the slight negatively charged PDA/PEI complex layer and negatively charged Cl^- ions, the applied electric field is sufficiently strong to overcome the electrostatic repulsion, allowing the Cl^- ions to pass through the PDA/PEI complex layer of the coated TFC NPMs. In contrast, ampicillin ions as model organics had a much smaller drift velocity of 2.2×10^{-6} Å fs^{-1} than Cl^- ions (drift velocity of 7.0×10^{-5} Å fs^{-1}), implying that the movement of ampicillin ions is not oriented towards a fixed pole, but rather they are almost stationary compared with the rapidly moving Cl^- ions (Supplementary Movie 3). Therefore, the movement of the ampicillin ions is not significantly influenced by the strong electric field applied. Due to the size exclusion effect, the ampicillin ions can be effectively retained by the PDA/PEI-coated NPMs and remained in the diluate side. Consequently, the ampicillin and Cl^- ions could be effectively separated. Therefore, the MD simulation further confirms the superiority of the electrodialytic separation performance using the PDA/PEI-coated TFC NPMs as ACMs for effective fractionation of organics and NaCl.

Generally, the conventional electrodialysis units equipped with AEMs are a platform technology for desalination of saline organic-rich solutions. However, the commercial AEMs (that is, AEM-5) suffered from serious membrane fouling for a 12-cycle electrodialytic separation operation during the fractionation of the antibiotics (that is, ceftriaxone sodium) and NaCl in the antibiotic/NaCl mixed solution (Supplementary Fig. 18). This was mainly attributed to the electrostatic attraction between negatively charged organics (that is, ceftriaxone ions) and positively charged quaternary ammonium group sites of the AEMs (Supplementary Fig. 18e), which can both induce pore blockage of the AEMs and substantially reduce the positive charge density of the AEMs (as reflected by remarkable boost in specific areal electric resistance of AEM-5 membrane after fouling in Supplementary Fig. 18d), which impedes the anion transfer. The fouling of the commercial AEM-5 membrane required an extended operation duration to remove the inorganic salts (that is, NaCl) from the feed (that is, diluate) for each cycle with a reduced desalination efficiency (Supplementary Fig. 18a). Specifically, the desalination efficiency of the commercial AEM-5 membrane declined from 98.0% to 97.5% in the ceftriaxone sodium/NaCl mixed solution after the 12-cycle electrodialytic separation operation. Correspondingly, the content of NaCl in the ceftriaxone

sodium/NaCl mixed solution was maintained at a level of >0.24 g l^{-1} at the 12-cycle separation operation (Supplementary Fig. 18b). On the other hand, negatively charged ceftriaxone ions inevitably transferred through the AEM-5 membrane to the concentrate side through electrostatic attraction under the electric field, resulting in high content of ceftriaxone sodium (>41 mg l^{-1}) in the concentrate side and low antibiotic recovery (<95.9%) (Supplementary Fig. 18c). Similarly, the AEM-5 membrane also experienced a deteriorating fractionation performance in the humic acid/NaCl mixed solution at an elevated salinity (~50 g l^{-1} NaCl), due to the fouling caused by humic acid during a four-cycle electrodialytic separation operation (Supplementary Fig. 19a). In particular, the AEM-5 membrane had a decreasing desalination efficiency from 98.9% to 98.6% (Supplementary Fig. 19b). Simultaneously, humic acid with a concentration of over 32 mg l^{-1} was observed in the concentrate, leading to a humic acid recovery of ca. 96.7% (Supplementary Fig. 19c). Consequently, the electrodialysis equipped with commercial AEMs as ACMs allows for the transfer of organics through the AEMs with a moderate loss of target organics, which is unfavourable for fractionation of organics and NaCl.

Therefore, utilization of bio-inspired PDA/PEI-coated TFC NPMs as ACMs in the electrodialytic separation process can facilitate the efficient one-step fractionation of the organics and inorganic salts (that is, NaCl) from saline organic-rich solutions containing antibiotics, remarkably outperforming the commercial AEMs. This proof-of-concept study sought to both effectively sieve the organic and inorganic salts for resource recovery from various saline organic-rich waste streams and provide guidelines for facile design of bespoken, cost-effective and high-performance ACMs to retrofit conventional high-fouling AEMs in the electro-driven separation applications for sustainable management of challenging waste stream.

Methods

Materials and chemicals

Commercially available, loose poly(piperazine-amide) TFC NPM (LNFM-1, MWCO 682 ± 17 Da) was purchased from Guangdong Yinachuan Environmental Technology, and was used as the substrate for fabrication of advanced ACMs. The commercial CEM (that is, CJMC-3) for cation transfer in electrodialysis was kindly supplied by ChemJoy Polymer Materials. Four commercial AEMs were supplied by Guangdong Yinachuan Environmental Technology, Shandong Tianwei Membrane Technology, Fumatech and ASTOM, which were designated as AEM-1 (AEM-N1), AEM-2 (TWEDA1R70), AEM-3 (FAS-30), AEM-4 (FAS-PET-130) and AEM-5 (Neosepta@AMX), respectively. Key properties of these commercial AEMs are presented in Supplementary Table 1.

PEI (average MW 600 Da, 99%) and tris(hydroxymethyl) aminomethane (Tris, >99%) were supplied by Shanghai Aladdin Biochemical Technology. Dopamine hydrochloride (>98%) was supplied from Sigma-Aldrich. These chemicals were used as received for surface coating of the loose NPM. Four antibiotics, that is, ceftriaxone sodium (MW 598.5 Da, >98%), cefotaxime sodium (MW 477.5 Da, 99.5%), carbenicillin disodium (MW 422.4 Da, USP grade) and ampicillin sodium (MW 371.4 Da, USP grade) were purchased from Shanghai Aladdin Biochemical Technology. NaCl (>99.0%) was supplied from Sigma-Aldrich. Chemicals were used as received without any purification.

Mussel-inspired coating of TFC NPMs

The mussel-inspired coating on the loose TFC NPM substrate was performed by co-deposition of dopamine and PEI as illustrated in Fig. 1a. The loose NPM substrate coupon was first loaded in the custom-made round mould, which allowed the membrane surface to stand with its side up. Subsequently, dopamine hydrochloride (2.0 g l^{-1}) and PEI (2.0 g l^{-1}) were homogeneously dissolved in a Tris buffer solution (50 mmol l^{-1}, pH 8.5) by vigorous stirring. Then, the as-prepared dopamine/PEI mixed solution was immediately poured into the mould for mussel-inspired surface coating onto the loose TFC NPM substrate. The co-deposition coating duration was fixed at 0, 6, 12, 18, 24, 30 and 36 h, respectively. The resulting membranes at variable coating durations were denoted as NPM-0 (pristine), NPM-1, NPM-2, NPM-3, NPM-4, NPM-5 and NPM-6, respectively.

Membrane characterization

The surface and cross-sectional morphologies of the membranes were visualized by SEM (NOVA NanoSEM 230; NOVA NanoSEM 450). The surface chemical composition of the membranes was recorded by X-ray photoelectron spectroscopy with Axis Supra+ spectrometer (Kratos Analytical). The selective layer thickness of the membranes was determined by AFM (Agilent 5500), as described in detail in Supplementary Information.

The surface hydrophilicity of the membranes was measured using an optical surface analyser (OSA200, Ningbo Scientific Instruments Company). The surface charge of the membranes was evaluated using an electrokinetic analyser (SurPASS, Anton Paar GmbH) in a 10.0 mmol l^{-1} NaCl electrolyte solution at pH 6.7 in terms of zeta potential. Specific areal electric resistance of the membranes was detected by a custom-designed four-compartment resistance analysis cell (ChemJoy Polymer Material) in a 0.5 mol l^{-1} NaCl solution, as illustrated in more detail in Supplementary Information. The pore size and MWCO of the membranes was measured by separation of 0.2 g l^{-1} poly(ethylene glycol) solutions with various MWs, as detailed in Supplementary Information.

Pressure-driven separation performance tests

The pressure-driven separation of the coated TFC NPMs was performed using a custom-designed cross-flow filtration unit at 4 bar and 25 ± 1 °C to evaluate their selectivity between the organics and the inorganic salt (that is, NaCl) (ref. 35). Initially, the TFC NPM coupon (effective area of 22.9 cm^2) was pre-pressurized by filtering the pure water at 6 bar to achieve a steady permeate flux. Subsequently, filtration of individual pure NaCl solutions with varying concentrations (that is, 1.0, 3.0, 7.5 and 12.0 g l^{-1}) or antibiotic solutions (that is, 1.0 g l^{-1} ceftriaxone sodium, cefotaxime sodium, carbenicillin disodium or ampicillin sodium) was conducted. Finally, separation of the antibiotic/NaCl mixed solutions with different NaCl concentrations (for example, up to 12.0 g l^{-1}) was conducted to evaluate the selectivity between the antibiotics and NaCl of the TFC NPMs. The rejection (R) of the solutes was calculated using equation (1):

$$R = \frac{C_f - C_p}{C_f} \quad (1)$$

where C_p and C_f are the concentration of antibiotics or NaCl present in the permeate and feed, respectively. The concentration of antibiotics was measured using a UV–vis spectrophotometer (Genesys 10S UV–vis spectrophotometer, Thermo Scientific)[36–39].

The selectivity (S) between Cl^- and the antibiotics for the TFC NPMs was calculated using equation (2)[40]:

$$S = \frac{1 - R_{NaCl}}{1 - R_{organics}} \quad (2)$$

where R_{NaCl} and $R_{organics}$ are the rejection of NaCl and antibiotics for the TFC NPMs when filtering the antibiotic/NaCl mixed solutions, respectively.

To fractionate the organics (that is, antibiotics) and NaCl by a pressure-driven separation process, a constant-volume nanofiltration-based diafiltration using a TFC NPM (that is, NPM-6) was conducted by the custom-designed cross-flow filtration system at 4 bar and 25 ± 1 °C (ref. 35). Specifically, a 300 ml organics/NaCl mixed solution (1.0 g l^{-1} organics and ~12 g l^{-1} NaCl) was used as feed. Pure water with various diavolume values (η, defined as the volume ratio between pure water

added and the feed during diafiltration) was added into the feed at an identical rate with the permeate to keep the feed volume unchanged.

The solute rejection (R_s) of the TFC NPMs during the constant-volume nanofiltration-based diafiltration procedure was determined by equation (1).

The recovery rate (α) of the organics during the constant-volume nanofiltration-based diafiltration was calculated using equation (3):

$$\alpha = \frac{C_{\text{final,organics}}}{C_{\text{initial,organics}}} \tag{3}$$

where $C_{\text{initial,organics}}$ and $C_{\text{final,organics}}$ represent the initial and final concentration of the antibiotic in the feed, respectively.

The desalination efficiency (β) of the constant-volume nanofiltration-based diafiltration was calculated using equation (4):

$$\beta = 1 - \frac{C_{\text{final,NaCl}}}{C_{\text{initial,NaCl}}} \tag{4}$$

where $C_{\text{initial,NaCl}}$ and $C_{\text{final,NaCl}}$ represent the initial and final concentration of NaCl in the feed, respectively.

Electrodialytic separation performance tests

The electro-driven separation performance of the PDA/PEI-coated TFC NPMs as ACMs were evaluated in a custom-designed electrodialysis cell (ChemJoy Polymer Material), where the AEMs were replaced for anion transfer to fractionate the organics/NaCl mixed solutions (Fig. 1b). The electrodialysis cell consisted of a cathode, an anode and a membrane stack (Supplementary Fig. 14a), where three pieces of the CEM coupons and two pieces of the TFC NPMs (effective area of 19.4 cm^2 for each membrane coupon) were alternatively inserted. A 0.3 mol l^{-1} Na_2SO_4 solution was used as an electrolyte in both cathode and anode chambers.

Initially, 300 ml pure NaCl solution (about 12 g l^{-1}) was used as the feed (diluate) in the electrodialytic separation at an applied current of 0.5 A to investigate the anion transfer capacity of the PDA/PEI coated TFC NPMs for desalination of pure NaCl solutions. The intermediate NaCl solution in the concentrate compartment had an identical salt concentration with the feed (diluate). To compare membrane performances of the surface-engineered TFC NPMs, four commercial AEMs (that is, AEM-1, AEM-2, AEM-3, AEM-4 and AEM-5) were applied as ACMs in the designed electrodialytic separation cell for desalination of pure NaCl solutions. When the conductivity of the feed decreased to 0.16 mS cm^{-1}, the electrodialytic separation operation was stopped immediately.

The energy consumption (E) and desalination efficiency (γ) of the electrodialytic separation process was determined by equations (5) and (6), respectively:

$$E = \int \frac{U \cdot I \cdot \mathrm{d}t}{\left(C^{\text{e}}_{\text{initial,NaCl}} - C^{\text{e}}_{\text{final,NaCl}}\right) \cdot V \cdot M} \tag{5}$$

$$\gamma = 1 - \frac{C^{\text{e}}_{\text{final,NaCl}}}{C^{\text{e}}_{\text{initial,NaCl}}} \tag{6}$$

where U is the applied voltage, I is the applied current, M is the molar mass of NaCl and V is the volume of the feed solution. $C^{\text{e}}_{\text{initial,NaCl}}$ and $C^{\text{e}}_{\text{final,NaCl}}$ represent the initial and final concentration of NaCl in the feed (diluate), respectively.

Subsequently, 300 ml antibiotic/NaCl (that is, ceftriaxone sodium/NaCl, cefotaxine sodium/NaCl, carbenicillin disodium/NaCl or ampicillin sodium/NaCl) mixed solutions (1.0 g l^{-1} antibiotic and ~12 g l^{-1} NaCl) were further used as feed in the electrodialytic separation process using the PDA/PEI-coated TFC NPMs (that is, NPM-6) as ACMs for fractionation of antibiotics and NaCl at a current of 0.5 A. During the desalination/fractionation of the antibiotic/NaCl mixed solutions, the electrodialytic separation process was terminated as the conductivity of the feed dropped below 0.2 mS cm^{-1}.

Finally, the fouling propensity of the PDA/PEI-coated TFC NPMs was investigated with an 18-cycle electrodialytic separation operation using the ceftriaxone sodium/NaCl mixed solution as feed to verify the stability of the surface-engineered TFC NPMs (that is, NPM-6) as ACMs for practical one-step fractionation of organics and NaCl. Simultaneously, the electrodialysis process equipped with the commercial AEMs (that is, AEM-5) was conducted using the ceftriaxone sodium/NaCl mixed solution as feed in the 12-cycle electrodialytic separation process under the same filtration conditions, highlighting the superiority of the surface-engineered TFC NPMs for fractionation of antibiotics and NaCl.

The desalination efficiency (γ) during the electrodialytic separation process for fractionation of antibiotics and NaCl was determined using equation (6).

The recovery rate (δ) of the antibiotics during the electrodialytic separation process for fractionation of antibiotics and NaCl was calculated using equation (7):

$$\delta = 1 - \frac{C^{\text{e}}_{\text{final,organics}}}{C^{\text{e}}_{\text{initial,organics}}} \tag{7}$$

where $C^{\text{e}}_{\text{initial,organics}}$ is the initial concentration of the antibiotics in the feed and $C^{\text{e}}_{\text{final,organics}}$ is the final concentration of the antibiotics in the concentrate compartment.

The permselectivity (P) between Cl^- and the antibiotics for the TFC NPMs during the electrodialytic separation process was calculated using equation (8)[41]:

$$P = \frac{\left(C^{\text{final}}_{\text{NaCl}} - C^{\text{initial}}_{\text{NaCl}}\right) \cdot C^{\text{final}}_{\text{organics}}}{\left(C^{\text{final}}_{\text{organics}} - C^{\text{initial}}_{\text{organics}}\right) \cdot C^{\text{final}}_{\text{NaCl}}} \tag{8}$$

where $C^{\text{initial}}_{\text{organics}}$ and $C^{\text{final}}_{\text{organics}}$ are the initial and final concentration of the antibiotics in the feed (diluate); $C^{\text{initial}}_{\text{NaCl}}$ and $C^{\text{final}}_{\text{NaCl}}$ is the initial and final concentration of NaCl in the feed (diluate) during the electrodialytic separation process.

Moreover, the desalination performance of the PDA/PEI-coated TFC NPMs (that is, NPM-6) as ACMs at was further tested with a four-cycle electrodialytic separation operation using the humic acid/NaCl mixed solution as feed to demonstrate their feasibility in one-step fractionation of humic acid and NaCl at the condition of higher salinity. Additionally, the commercial AEMs (that is, AEM-5) was equipped for desalination performance comparison with the surface-engineered TFC NPMs for fractionation of humic acid and NaCl. Specifically, 300 ml humic acid/NaCl mixed solution (1.0 g l^{-1} humic acid and ~50 g l^{-1} NaCl) were used as feed in the electrodialytic separation process using both NPM-6 and AEM-5 as ACMs for fractionation of humic acid and NaCl at a current of 0.8 A. It is worth noting that the required energy consumption increases and diluate quality deteriorates with increasing salinity of the feed during the electrodialysis process, due to the back diffusion of counter ions[42]. It is demonstrated that the electrodialysis is more cost-effective desalination system at the low salinity[43]. Therefore, the salinity of the humic acid/NaCl mixed solution was set at the level of 50 g l^{-1} in this case, which can be sufficient to demonstrate the desalination performance of the ACMs at the condition of elevated salinity.

MD simulation

To explore the mass transport mechanism of the PDA/PEI-coated TFC NPMs in electrodialysis, we simulated the transfer behaviour of different ions (that is, Cl^-, Na^+ and ampicillin ions) under an applied electric

field through MD. A more detailed description of the MD simulation can be found in Supplementary Information.

Data availability

The authors declare that the main data supporting the findings of this study are contained within the paper. Key, unprocessed experimental datasets for Figs. 1, 2 and 5 are available in Figshare (https://doi.org/10.6084/m9.figshare.21900870). All other relevant data are available from the corresponding author upon reasonable request.

References

1. McCarty, P. L., Bae, J. & Kim, J. Domestic wastewater treatment as a net energy producer—can this be achieved? *Environ. Sci. Technol.* **45**, 7100–7106 (2011).
2. Logan, B. E. & Rabaey, K. Conversion of wastes into bioelectricity and chemicals by using microbial electrochemical technologies. *Science* **337**, 686–690 (2012).
3. DuChanois, R. M. et al. Designing polymeric membranes with coordination chemistry for high-precision ion separations. *Sci. Adv.* **8**, m9436 (2022).
4. Yao, Y. et al. High performance polyester reverse osmosis desalination membrane with chlorine resistance. *Nat. Sustain.* **4**, 138–146 (2021).
5. Zuo, K. et al. Multifunctional nanocoated membranes for high-rate electrothermal desalination of hypersaline waters. *Nat. Nanotechnol.* **15**, 1025–1032 (2020).
6. Lin, J. et al. Integrated loose nanofiltration-electrodialysis process for sustainable resource extraction from high-salinity textile wastewater. *J. Hazard. Mater.* **419**, 126505 (2021).
7. Ye, W. et al. Sustainable management of landfill leachate concentrate through recovering humic substance as liquid fertilizer by loose nanofiltration. *Water Res.* **157**, 555–563 (2019).
8. Ahmad, N. N. R., Ang, W. L., Leo, C. P., Mohammad, A. W. & Hilal, N. Current advances in membrane technologies for saline wastewater treatment: a comprehensive review. *Desalination* **517**, 115170 (2021).
9. Mandeep, Gupta Kumar, G. & Shukla, P. Insights into the resources generation from pulp and paper industry wastes: challenges, perspectives and innovations. *Bioresource Technol.* **297**, 122496 (2020).
10. Zhang, X. Selective separation membranes for fractionating organics and salts for industrial wastewater treatment: design strategies and process assessment. *J. Membr. Sci.* **643**, 120052 (2022).
11. Lu, Y. et al. Two-dimensional fractal nanocrystals templating for substantial performance enhancement of polyamide nanofiltration membrane. *Proc. Natl Acad. Sci. USA* **118**, e2019891118 (2021).
12. Liang, Y. et al. Polyamide nanofiltration membrane with highly uniform sub-nanometre pores for sub-1 Å precision separation. *Nat. Commun.* **11**, 2015 (2020).
13. Zhang, W. et al. General synthesis of ultrafine metal oxide/reduced graphene oxide nanocomposites for ultrahigh-flux nanofiltration membrane. *Nat. Commun.* **13**, 471 (2022).
14. Wang, Z. et al. Nanoparticle-templated nanofiltration membranes for ultrahigh performance desalination. *Nat. Commun.* **9**, 2004 (2018).
15. Shen, L. et al. Polyamide-based membranes with structural homogeneity for ultrafast molecular sieving. *Nat. Commun.* **13**, 500 (2022).
16. Feng, X. et al. Precise nanofiltration in a fouling-resistant self-assembled membrane with water-continuous transport pathways. *Sci. Adv.* **5**, v9308 (2019).
17. Lin, J. et al. Unraveling flux behavior of superhydrophilic loose nanofiltration membranes during textile wastewater treatment. *J. Membr. Sci.* **493**, 690–702 (2015).
18. Guo, Y., Li, T., Xiao, K., Wang, X. & Xie, Y. F. Key foulants and their interactive effect in organic fouling of nanofiltration membranes. *J. Membr. Sci.* **610**, 118252 (2020).
19. Lee, S., Cho, J. & Elimelech, M. Combined influence of natural organic matter (NOM) and colloidal particles on nanofiltration membrane fouling. *J. Membr. Sci.* **262**, 27–41 (2005).
20. Wang, X., Zhang, C. & Ouyang, P. The possibility of separating saccharides from a NaCl solution by using nanofiltration in diafiltration mode. *J. Membr. Sci.* **204**, 271–281 (2002).
21. Al-Amshawee, S. et al. Electrodialysis desalination for water and wastewater: a review. *Chem. Eng. J.* **380**, 122231 (2020).
22. Xu, T. & Huang, C. Electrodialysis-based separation technologies: a critical review. *AIChE J* **54**, 3147–3159 (2008).
23. Patel, S. K., Qin, M., Walker, W. S. & Elimelech, M. Energy efficiency of electro-driven brackish water desalination: electrodialysis significantly outperforms membrane capacitive deionization. *Environ. Sci. Technol.* **54**, 3663–3677 (2020).
24. Xue, C. et al. Acid blue 9 desalting using electrodialysis. *J. Membr. Sci.* **493**, 28–36 (2015).
25. Lee, H., Hong, M., Han, S., Cho, S. & Moon, S. Fouling of an anion exchange membrane in the electrodialysis desalination process in the presence of organic foulants. *Desalination* **238**, 60–69 (2009).
26. Hansima, M. A. C. K. et al. Fouling of ion exchange membranes used in the electrodialysis reversal advanced water treatment: a review. *Chemosphere* **263**, 127951 (2021).
27. Yang, H. et al. Dopamine: just the right medicine for membranes. *Adv. Funct. Mater.* **28**, 1705327 (2018).
28. Lee, H., Dellatore, S. M., Miller, W. M. & Messersmith, P. B. Mussel-inspired surface chemistry for multifunctional coatings. *Science* **318**, 426–430 (2007).
29. Qiu, W., Yang, H. & Xu, Z. Dopamine-assisted co-deposition: an emerging and promising strategy for surface modification. *Adv. Colloid Interfaces Sci.* **256**, 111–125 (2018).
30. Ponzio, F. et al. Oxidant control of polydopamine surface chemistry in acids: a mechanism-based entry to superhydrophilic-superoleophobic coatings. *Chem. Mater.* **28**, 4697–4705 (2016).
31. Teixeira, M. R., Rosa, M. J. & Nyström, M. The role of membrane charge on nanofiltration performance. *J. Membr. Sci.* **265**, 160–166 (2005).
32. Childress, A. E. & Elimelech, M. Relating nanofiltration membrane performance to membrane charge (electrokinetic) characteristics. *Environ. Sci. Technol.* **34**, 3710–3716 (2000).
33. Jun, B. et al. Charge characteristics (surface charge vs. zeta potential) of membrane surfaces to assess the salt rejection behavior of nanofiltration membranes. *Sep. Purif. Technol.* **247**, 117026 (2020).
34. Richards, L. A., Vuachère, M. & Schäfer, A. I. Impact of pH on the removal of fluoride, nitrate and boron by nanofiltration/reverse osmosis. *Desalination* **261**, 331–337 (2010).
35. Lin, J. et al. Fractionation of direct dyes and salts in aqueous solution using loose nanofiltration membranes. *J. Membr. Sci.* **477**, 183–193 (2015).
36. Yang, J. & Luo, X. Ag-doped TiO_2 immobilized cellulose-derived carbon beads: one-pot preparation, photocatalytic degradation performance and mechanism of ceftriaxone sodium. *Appl. Surf. Sci.* **542**, 148724 (2021).
37. Li, T. et al. Highly efficient photoelectrocatalytic degradation of cefotaxime sodium on the $MoSe_2/TiO_2$ nanotubes photoanode with abundant oxygen vacancies. *J. Solid State Chem.* **303**, 122455 (2021).

38. Olad, A. & Nosrati, R. Use of response surface methodology for optimization of the photocatalytic degradation of ampicillin by ZnO/polyaniline nanocomposite. *Res. Chem. Intermed.* **41**, 1351–1363 (2015).
39. Lin, C., Wang, Y., Shen, L. & Lin, C. The dentin permeability of anti-inflammatory and antibacterial drugs: in vitro study. *J. Formos. Med. Assoc* **118**, 828–832 (2019).
40. Liu, T. et al. Ion-responsive channels of zwitterion-carbon nanotube membrane for rapid water permeation and ultrahigh mono-/multivalent ion selectivity. *ACS Nano* **9**, 7488–7496 (2015).
41. Lan, Y. et al. A monovalent selective anion exchange membrane made by poly(2,6-dimethyl-1,4-phenyl oxide) for bromide recovery. *Sep. Purif. Technol.* **305**, 122337 (2023).
42. Yan, H. et al. Multistage-batch electrodialysis to concentrate high-salinity solutions: process optimisation, water transport, and energy consumption. *J. Membr. Sci.* **570-571**, 245–257 (2019).
43. Shah, K. M. et al. Drivers, challenges, and emerging technologies for desalination of high-salinity brines: a critical review. *Desalination* **538**, 115827 (2022).

Acknowledgements

This work was financially supported by the National Key Research and Development Program of China (2021YFC3201400), the Natural Science Foundation of Fujian Province (2021J01628), the Fujian Provincial Department of Science and Technology (2019Y0006), the Royal Society (IEC\NSFC\211021), the Royal Academy of Engineering (IF2223B-104) and the Leverhulme Trust (RPG-2022-177). Y.M.L. appreciates the financial support from Korea Institute of Energy Technology Evaluation and Planning (KETEP) grant (20202020800330). D.H.S acknowledges the support of Korea Institute of Energy Technology Evaluation and Planning (KETEP) and the Ministry of Trade, Industry & Energy (MOTIE) of the Republic of Korea (no. 20224000000100). The computational work for this article was (fully/partially) performed on resources of the National Supercomputing Centre (NSCC), Singapore (https://www.nscc.sg). R. Zhang and H. Chang from Hebei University of Technology, China, are thanked for AFM and SEM imaging measurements.

Author contributions

J.L., W.Y., M.X. and Y.M.L. conceived the idea and designed the research. J.L., W.Y., S.X., J.D., R.L., X.C. and Z.Y. prepared the PDA/PEI-coated TFC NPMs and performed the pressure-driven and electro-driven separation experiments. E.Y.M.A., W.T., D.D.H. and T.Y.N. performed the MD simulation. J.L., W.Y., D.Z., S.F., D.H.S., S.Z., B.V.D.B., M.X. and Y.M.L. contributed to interpreting the data and writing the manuscript.

Competing interests

The authors declare that they have no competing interests.

Additional information

Supplementary information The online version contains supplementary material available at https://doi.org/10.1038/s44221-023-00113-5.

Correspondence and requests for materials should be addressed to Jiuyang Lin, Wenyuan Ye, Ming Xie or Young Moo Lee.

Peer review information *Nature Water* thanks Kyoung Jin Alicia An and the other, anonymous, reviewer for their contribution to the peer review of this work.